Ab initio study of mode-resolved phonon transmission at Si/Ge interfaces using atomistic Green's functions

Benoit Latour, Nina Shulumba, and Austin J. Minnich*

Division of Engineering and Applied Science, California Institute of Technology, Pasadena, California 91125, USA

(Received 27 May 2017; revised manuscript received 9 August 2017; published 25 September 2017)

Solid interfaces with exceptionally low or high thermal conductance are of intense scientific and practical interest. However, realizing such interfaces is challenging due to a lack of knowledge of the phonon transmission coefficients between specific modes on each side of the interface and how the coefficients are affected by atomic scale structure. Here, we report an *ab initio* based study of phonon transmission at Si/Ge interfaces using a recent extension of the atomistic Green's function method that resolves transmission coefficients by mode. These results provide a detailed framework to investigate the precise transmission and reflection processes that lead to thermal resistance and how they depend on phonon frequency as well as incident angle. We find that the transmission and reflection processes can be partly explained with familiar concepts such as conservation of transverse momentum, but we also find that numerous phonons have zero transmission coefficient despite the existence of modes that satisfy transverse momentum conservation. This work provides detailed insights into precisely which phonons transmit or reflect at interfaces, knowledge necessary to design solid interfaces with extreme values of thermal conductance for thermoelectricity and heat management applications.

DOI: 10.1103/PhysRevB.96.104310

I. INTRODUCTION

Two-dimensional defects, such as heteregenous interfaces or grain boundaries, play a key role in the overall properties of nanomaterials [1]. In contrast to what has been achieved with photons or electrons, the understanding of phonon transmission processes at solid interfaces remains poorly developed, with direct measurements of transmission coefficients having only been recently reported [2]. Therefore, designing interfaces with extreme values of thermal boundary resistance (TBR) is still a challenge. Crucial technologies, such as thermal interface materials [3] or thermoelectrics [4,5], would greatly benefit from a better understanding of phonon transmission through two-dimensional defects.

To achieve such a control over TBR, knowledge of transmission coefficients for all phonons over the Brillouin zone is essential, exactly as knowledge of Fresnel coefficients is essential for designing optical antireflection coatings. However, most analytical models and computational tools do not provide this detailed information. Simple models such as the acoustic mismatch model (AMM) in the long wavelength limit and the diffuse mismatch model (DMM) in the short wavelength limit fail to reproduce many experimental observations [6]. Molecular dynamics simulations [7,8] have allowed the overall value of the TBR to be computed, including the full anharmonicity of the interatomic potential. Mode-resolved techniques [9–14] were recently developed to investigate how specific phonon modes are affected by interfaces. However, the typical wave packet approach is extremely computationally expensive for many modes in a Brillouin zone grid.

The atomistic Green's function (AGF) method [15] has also been used extensively to compute the transmission through a device connected to reservoirs given knowledge of the empirical or *ab initio* force constants. While the original AGF algorithm [16–23] yields transmission coefficients that are resolved only by phonon frequency, recently Ong and Zhang [24] extended the AGF formalism for mode-resolved calculations on a graphene/boron-nitride interface using empirical force constants. A similar numerical method [25] based on the harmonic force constants has also been developed using perfectly matched layer boundaries to compute mode-resolved transmission. However, these algorithms have not yet been applied to interfaces between three-dimensional solids with *ab initio* force constants.

In this work, we have investigated interfacial phonon transmission using the mode-resolved AGF formalism for a Si/Ge interface with force constants obtained from first principles. In Sec. II, we present the methodology with the mode-resolved formalism of the AGF, which allows for the calculation of transmission coefficients from a specific mode in a material to a specific mode in the other material. After, we obtain the modal transmission coefficients and analyze the results, particularly in comparison to the predictions of simple models like the AMM. Finally, we examine the zero-transmission processes to draw general conclusions on the physical mechanisms involved in the phonon transmission.

II. METHODOLOGY

We first briefly describe the formalism used to compute the mode-resolved transmission coefficients as reported in Ref. [24]. This method requires knowledge of the harmonic force constants of the system, which we obtain from first principles using the temperature-dependent effective potential method (TDEP) [26–28].

A. Original atomistic Green's functions

In the original framework of the AGF [15,29], the studied system is divided into three interacting parts: the left and right semi-infinite leads and the device, as depicted in Fig. 1. It is possible to write the equation of motion of this system using

*aminnich@caltech.edu

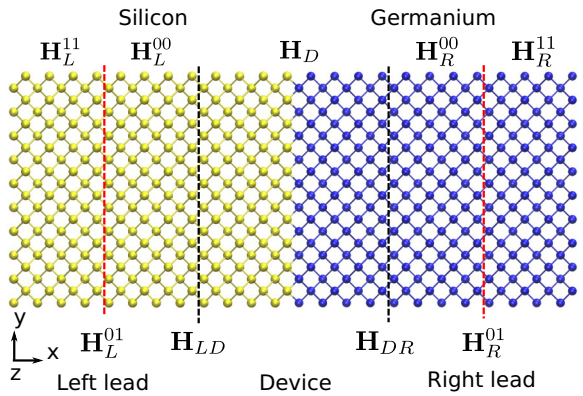

FIG. 1. Atomic structure of the Si/Ge interface. The black dashed lines separate the system into three subsystems: the left (Si) and right (Ge) semi-infinite leads and the device containing the interface. For each lead, two identical layers are created (red dashed lines) for the mode-resolved AGF formalism.

the following matrix form:

$$(\omega^2\mathbf{I} - \mathbf{H})\Psi = 0, \tag{1}$$

where ω is the radial frequency, $\mathbf{I}$ is the identity matrix, Ψ are the eigenvectors of the total system, and $\mathbf{H}$ is the harmonic matrix representing the atomic interactions,

$$\mathbf{H} = \left[\begin{array}{ccc|c|ccc} \ddots & \vdots & \vdots & & & & \\ \cdots & \mathbf{H}_L^{11} & \mathbf{H}_L^{01} & \mathbf{0} & & & \\ \cdots & \mathbf{H}_L^{10} & \mathbf{H}_L^{00} & \mathbf{H}_{LD} & & & \\ \hline & \mathbf{0} & \mathbf{H}_{DL} & \mathbf{H}_D & \mathbf{H}_{DR} & \mathbf{0} & \\ \hline & & \mathbf{0} & \mathbf{H}_{RD} & \mathbf{H}_R^{00} & \mathbf{H}_R^{01} & \cdots \\ & & & \vdots & \mathbf{H}_R^{10} & \mathbf{H}_R^{11} & \cdots \\ & & & & \vdots & \vdots & \ddots \end{array}\right], \tag{2}$$

where $\mathbf{H}_D$ is the harmonic matrix of the device, $\mathbf{H}_{LD}$ is the coupling matrix between the left lead and the device, and $\mathbf{H}_{DR}$ the coupling matrix between the device and the right lead. As $\mathbf{H}$ is Hermitian, $\mathbf{H}_{LD} = \mathbf{H}_{DL}^\dagger$ and $\mathbf{H}_{RD} = \mathbf{H}_{DR}^\dagger$. The harmonic matrix of the left lead $\mathbf{H}_L$ is divided into submatrices, where $\mathbf{H}_L^{00}$ represents the harmonic matrix of the layer in the left lead in contact with the device, $\mathbf{H}_L^{11}$ the harmonic matrix of the layer in the left lead in contact with the previous layer, and $\mathbf{H}_L^{01}$ the coupling matrix between them, as depicted in Fig. 1. The same notation is also used for the right lead. The device retarded Green's function $\mathbf{G}_D^{\text{ret}}(\omega)$ is defined as

$$\mathbf{G}_D^{\text{ret}}(\omega) = (\omega^2\mathbf{I} - \mathbf{H}_D - \Sigma_L - \Sigma_R)^{-1}, \tag{3}$$

where $\Sigma_{L,R}$ are the self-energies of the left and right leads respectively, representing the coupling between the leads and the device. They are defined using the left and right uncoupled retarded Green's functions $\mathbf{g}_L^{00} = [(\omega^2 + \eta i)\mathbf{I} - \mathbf{H}_L]^{-1}$ and $\mathbf{g}_R^{00} = [(\omega^2 + \eta i)\mathbf{I} - \mathbf{H}_R]^{-1}$, which are computed with the decimation technique [30], each lead being divided into two equivalent sublayers, as depicted in Fig. 1. We checked that $\eta = 10^{-6}\omega^2$ is small enough not to affect the density of states and guarantee a quick convergence of the decimation technique. The self-energies are defined as $\Sigma_L = \mathbf{H}_{DL}\mathbf{g}_L^{00}\mathbf{H}_{LD}$ and $\Sigma_R = \mathbf{H}_{DR}\mathbf{g}_R^{00}\mathbf{H}_{RD}$. The transmission spectrum is finally calculated using the Caroli formula:

$$\Xi(\omega) = \text{Tr}(\Gamma_R\mathbf{G}^{\text{ret}}\Gamma_L\mathbf{G}^{\text{ret}\,\dagger}), \tag{4}$$

with $\Gamma_L = i(\Sigma_L - \Sigma_L^\dagger)$ and $\Gamma_R = i(\Sigma_R - \Sigma_R^\dagger)$. Finally, the thermal conductance $G(T)$ is computed using the Landauer formalism:

$$G(T) = \frac{1}{2\pi A}\int_0^{+\infty} \hbar\omega\frac{\partial n}{\partial T}(\omega,T)\Xi(\omega)d\omega, \tag{5}$$

with $n(\omega,T)$ the Bose-Einstein distribution and A the transverse area. For the Si/Ge interface, the equation for the thermal conductance is modified as described by Tian *et al.* [19]. To reduce the computation time for the transverse directions, a Fourier transform of the equations of motion in both transverse directions is carried out and the transmission $\Xi(\omega,\vec{k}_\parallel)$ is computed for each transverse wave vector $\vec{k}_\parallel$ defined on a uniform grid: $\Xi(\omega) = 1/N_{\vec{k}_\parallel}\sum_{\vec{k}_\parallel}\Xi(\omega,\vec{k}_\parallel)$, where $N_{\vec{k}_\parallel}$ is the number of transverse wave vectors.

B. Mode-resolved atomistic Green's functions

We now present the mode-resolved AGF formalism adapted by Ong *et al.* [24] from electronic transport [31]. This theory is based on Bloch matrices using the translational symmetry in both left and right leads. These matrices give for each mode in both leads the phase change of the eigenvectors passing from one unit cell to the neighbor. The Bloch matrices for modes traveling from the left to right leads can be defined from the uncoupled retarded Green's functions $\mathbf{g}_L^{00}$ and $\mathbf{g}_R^{00}$:

$$\mathbf{F}_L^{\text{adv}} = \left[\left(\mathbf{H}_L^{10}\mathbf{g}_L^{00}\right)^\dagger\right]^{-1}, \tag{6}$$

$$\mathbf{F}_R^{\text{ret}} = \mathbf{g}_R^{00}\mathbf{H}_R^{10}. \tag{7}$$

The diagonalization of these Bloch matrices provides the eigenvector matrices $\{\mathbf{U}_L^{\text{adv}},\mathbf{U}_R^{\text{ret}}\}$ in both leads associated with eigenvalue matrices $\Lambda_L^{\text{adv}},\Lambda_R^{\text{ret}}$ corresponding to a phase factor $e^{ik_\perp a}$, where a represents the sublayer thickness in each lead, and $k_\perp$ is the longitudinal component of the wave vector:

$$\mathbf{F}_L^{\text{adv}}\mathbf{U}_L^{\text{adv}} = \Lambda_L^{\text{adv}}\mathbf{U}_L^{\text{adv}}, \tag{8}$$

$$\mathbf{F}_R^{\text{ret}}\mathbf{U}_R^{\text{ret}} = \Lambda_R^{\text{ret}}\mathbf{U}_R^{\text{ret}}. \tag{9}$$

Two groups of modes can be created from this diagonalization: propagating phonons with $|\Lambda_{nn}| = 1$ and evanescent modes with $|\Lambda_{nn}| < 1$, where n is the index of the phonon mode. We only consider in the following the propagating modes. The knowledge of the longitudinal component of the wave vector, in addition to the transverse ones involved in the transverse Fourier transform of the equations of motion, provides the angle between the phonon wave vector and the heat flux direction. It is important to note that the number of propagating modes corresponds to the number of branches at a specific frequency and transverse wave vector, which can be zero. The velocity matrices $\mathbf{V}_L$ and $\mathbf{V}_R$ are also necessary to compute

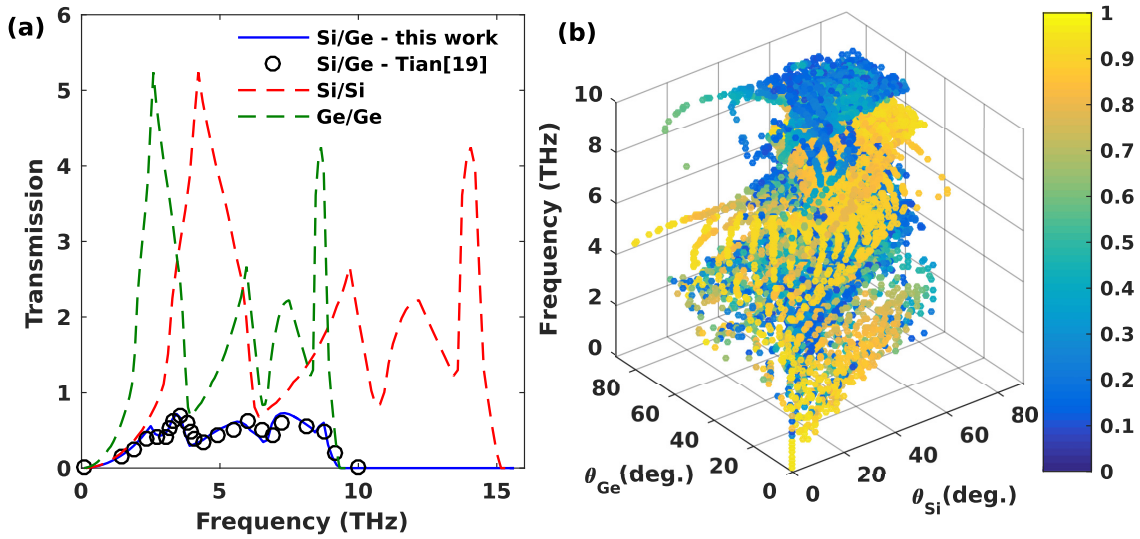

FIG. 2. (a) Transmission versus phonon frequency through the Si/Ge interface obtained from the AGF compared to the results of Tian *et al.* [19] (open circles). The transmission spectra through bulk Si (red dashed) and Ge (green dashed) are plotted to show the effect of the Si/Ge interface on the phonon transport on the whole spectrum. (b) Mode-resolved transmission as a function of frequency, angle of the phonon in Si, θ_{Si}, and angle in Ge, θ_{Ge}. The colormap indicates the transmission coefficient for each pair of modes from Si and Ge leads, from 0 (dark blue) to 1 (yellow).

the mode-resolved transmission coefficients:

$$\mathbf{V}_L = \frac{a_L}{2\omega}\mathbf{U}_L^{\mathrm{adv}\,\dagger}\Gamma_L^{00}\mathbf{U}_L^{\mathrm{adv}}, \tag{10}$$

$$\mathbf{V}_R = \frac{a_R}{2\omega}\mathbf{U}_R^{\mathrm{ret}\,\dagger}\Gamma_R^{00}\mathbf{U}_R^{\mathrm{ret}}, \tag{11}$$

with $\Gamma_L^{00} = i(\Sigma_L^{00} - \Sigma_L^{00\dagger})$, $\Gamma_R^{00} = i(\Sigma_R^{00} - \Sigma_R^{00\dagger})$, $\Sigma_L^{00} = \mathbf{H}_L^{10}\mathbf{g}_L^{00}\mathbf{H}_L^{01}$, $\Sigma_R^{00} = \mathbf{H}_R^{01}\mathbf{g}_R^{00}\mathbf{H}_R^{10}$, and $a_{L,R}$ the sublayer thicknesses of the left and right leads respectively. $\mathbf{V}_L$ and $\mathbf{V}_R$ respectively correspond to the projection of the mode group velocity in the left and right leads along the temperature gradient direction, so they are null for evanescent phonons. Finally, the mode-resolved transmission matrix $\mathbf{t}$ is computed as

$$\mathbf{t} = \frac{2i\omega}{\sqrt{a_L a_R}}\mathbf{V}_R^{1/2}\left[\mathbf{U}_R^{\mathrm{ret}}\right]^{-1}\mathcal{G}^{\mathrm{ret}}\left[\mathbf{U}_L^{\mathrm{adv}\,\dagger}\right]^{-1}\mathbf{V}_L^{1/2} \tag{12}$$

with

$$\mathcal{G}^{\mathrm{ret}} = \mathbf{g}_R^{00}\mathbf{H}_{RD}\mathbf{G}_D^{\mathrm{ret}}\mathbf{H}_{DL}\mathbf{g}_L^{00}. \tag{13}$$

This matrix provides the transmission for each mode of the left lead coupled with phonons in the right lead and the eigenvalue matrices Λ_L^{adv} and Λ_R^{ret}, the information about the angle of each wave vector with the heat flux direction. The element $|t_{ij}|^2$ provides the transmission coefficient for a mode i in the left lead coupled with phonon j in the right lead, and $\alpha_i = \sum_j |t_{ij}|^2$ the transmission for a mode i in the left lead to all possible modes in the right lead.

III. MODE-RESOLVED TRANSMISSION COEFFICIENTS THROUGH A Si/Ge INTERFACE

A. Description of the Si/Ge interface

We apply the mode-resolved AGF formalism to a Si/Ge interface. The structure of the studied system is shown in Fig. 1. We assume identical interactions between Si and Ge atoms based on the *ab initio* force constants of bulk silicon [28]. The mass mismatch between the two materials is considered as the key parameter for phonon reflection and transmission at the interface [20]. The heat flux direction x is oriented along the [100] direction of the conventional cell of bulk silicon. The atomic masses of Si and Ge atoms are respectively set to 27.98 and 73.92 amu. As the interaction cutoff has been set to 9.42 Å, the thickness of each layer in the left and right leads is equal to twice the lattice constant of bulk Si, 10.88 Å. We used periodic boundary conditions and Fourier transformed the dynamical equation in the transverse directions. We set the transverse k point grid to 100×100 to ensure the convergence of the transmission spectrum with respect to the transverse size. We also used the SPGLIB code library to consider the irreducible k points of the structure.

B. Angular transmission spectrum of the Si/Ge interface

The transmission spectrum through the Si/Ge interface, obtained from the traditional AGF formalism, is plotted in Fig. 2(a). This result is compared with the transmission spectra through bulk Si and Ge for which no interface exists. Until 2 THz, low frequency phonons transmit through the Si/Ge interface with a transmission close to the one in Si bulk, as it is the material with the limiting transmission. The higher frequency phonons reflect at the interface with a much higher probability as they are affected by the atomic mass mismatch between the two materials. The Si/Ge spectra are consistent with that computed for a perfect Si/Ge interface *ab initio* by Tian *et al.* [19]; the interface conductance G we obtain is 2.10×10^8 W m^{-2}K^{-1} at 300 K, in good agreement with the value of 2.09×10^8 W m^{-2}K^{-1} calculated by Tian *et al.*

We now use the mode-resolved AGF formalism to compute the transmission coefficients for a mode in the left reservoir

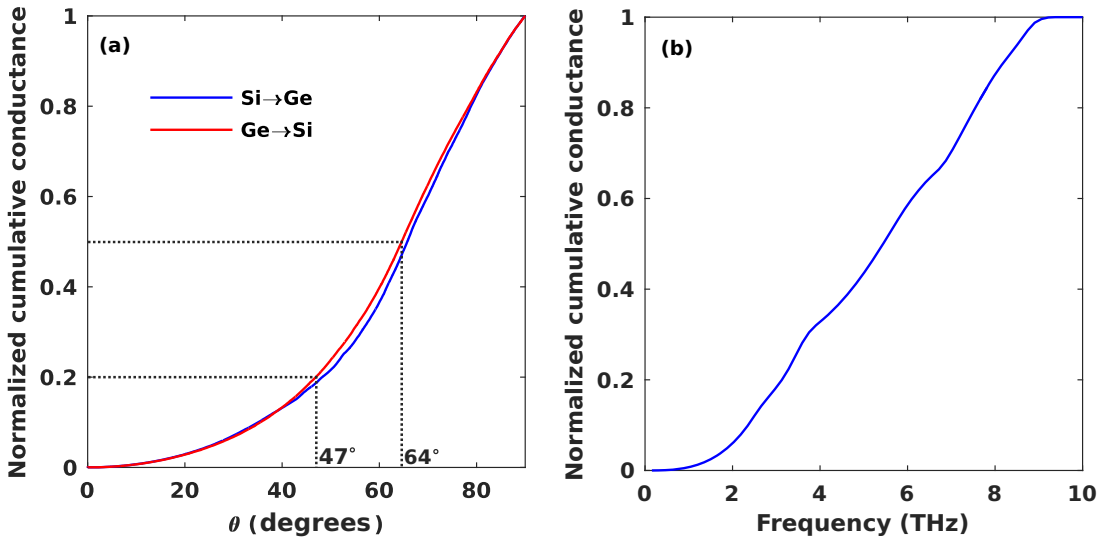

FIG. 3. Cumulative interface thermal conductance. (a) As a function of angle of incidence in Si and Ge $C_G(\theta)$. Phonons with incidence angle greater than 45° contribute to 80% of the TBR. (b) As a function of frequency $C_G(\omega)$. The whole phonon spectrum contributes almost uniformly to the TBR.

to another mode in the right reservoir for various frequencies and transverse components of the wave vector. Figure 2(b) presents the transmission coefficient for each pair of modes from Si and Ge leads as a function of frequency and the angle of these modes in each material with respect to the normal to the interface. We observe several general trends, including that low frequency phonons have transmission coefficients near unity and that modes with large incident angles are likely to reflect. It is worth noting that individual phonons can still transmit with a near perfect transmission close to the cutoff frequency of Ge density of states at 9 THz. Besides these general observations, the coefficients vary widely, and therefore additional analysis is required to extract useful information from this large dataset to identify the physical principles governing the transmission processes.

To begin, we examine the cumulative thermal conductance as a function of the incident angle $C_G(\theta)$ and frequency $C_G(\omega)$ from both Si and Ge leads. These quantities are defined as

$$C_G(\theta) = \frac{\int_0^{\theta}\left(\int_0^{\omega_{\max}} G(\theta,\omega)d\omega\right)d\theta}{\int_0^{\pi/2}\left(\int_0^{\omega_{\max}} G(\theta,\omega)d\omega\right)d\theta}, \tag{14}$$

$$C_G(\omega) = \frac{\int_0^{\omega}\left(\int_0^{\pi/2} G(\theta,\omega)d\theta\right)d\omega}{\int_0^{\omega_{\max}}\left(\int_0^{\pi/2} G(\theta,\omega)d\theta\right)d\omega}, \tag{15}$$

where $\omega_{\max}$ is the maximum frequency in the system, θ the incident angle and $G(\theta,\omega)$ the thermal conductance for each mode. Figure 3(a) shows that a broad range of incident angles contribute to the total thermal conductance: 80% is due to incident phonons with an incident angle larger than 47° and 50% for incident angle larger than 64°. This result is partially explained by the large number of incident modes with a high incident angle and leads to a key conclusion: dramatically modifying the TBR requires affecting phonons with incident angle larger than 45°.

The frequency-dependent cumulative thermal conductance $C_G(\omega)$ is plotted in Fig. 3(b). Again, a broad range of the phonon spectrum contributes to the TBR between 1 and 9 THz. This is due to the weak dependence of the transmission spectrum of Fig. 2(b) as a function of frequency. This result indicates that achieving extreme values of TBR requires consideration of the entire phonon spectrum over a wide range of frequencies.

C. Comparison with the acoustic mismatch model

We next examine how our calculations compare with the widely used AMM, which is expected to be valid in the low frequency limit. The AMM is based on the assumption of elastic wave theory in which acoustic waves propagate through a continuous medium characterized by an acoustic impedance $Z = \rho v$, where ρ represents the volumetric mass density of the material and v the speed of sound in the material. The acoustic impedance mismatch at the interface can lead to either a phonon reflection or transmission possibly involving mode conversion. Conservation of the transverse components of the wave vector at the interface leads to Snell's law when mode conversion is not considered in an isotropic medium:

$$\frac{\sin\theta_1}{v_1} = \frac{\sin\theta_2}{v_2}, \tag{16}$$

where θ_1 and θ_2 are the incident and reflected/transmitted angles with respect to the normal vector of the surface, respectively. In the following, we consider a simplified model for the mode conversion at the interface, which provides analytical equations for both Snell's law and the phonon transmission through the Si/Ge interface. Thus, we can express the transmission in the AMM as follows:

$$t_{\mathrm{AMM}} = \frac{4Z_1Z_2\cos\theta_1\cos\theta_2}{(Z_1\cos\theta_1 + Z_2\cos\theta_2)^2}. \tag{17}$$

These two equations are applied to three ideal cases where (1) longitudinal (respectively transverse) phonons are transmitted as longitudinal (resp. transverse) phonons, corresponding to no mode conversion (noted as $T \to T$ and $L \to L$), (2)

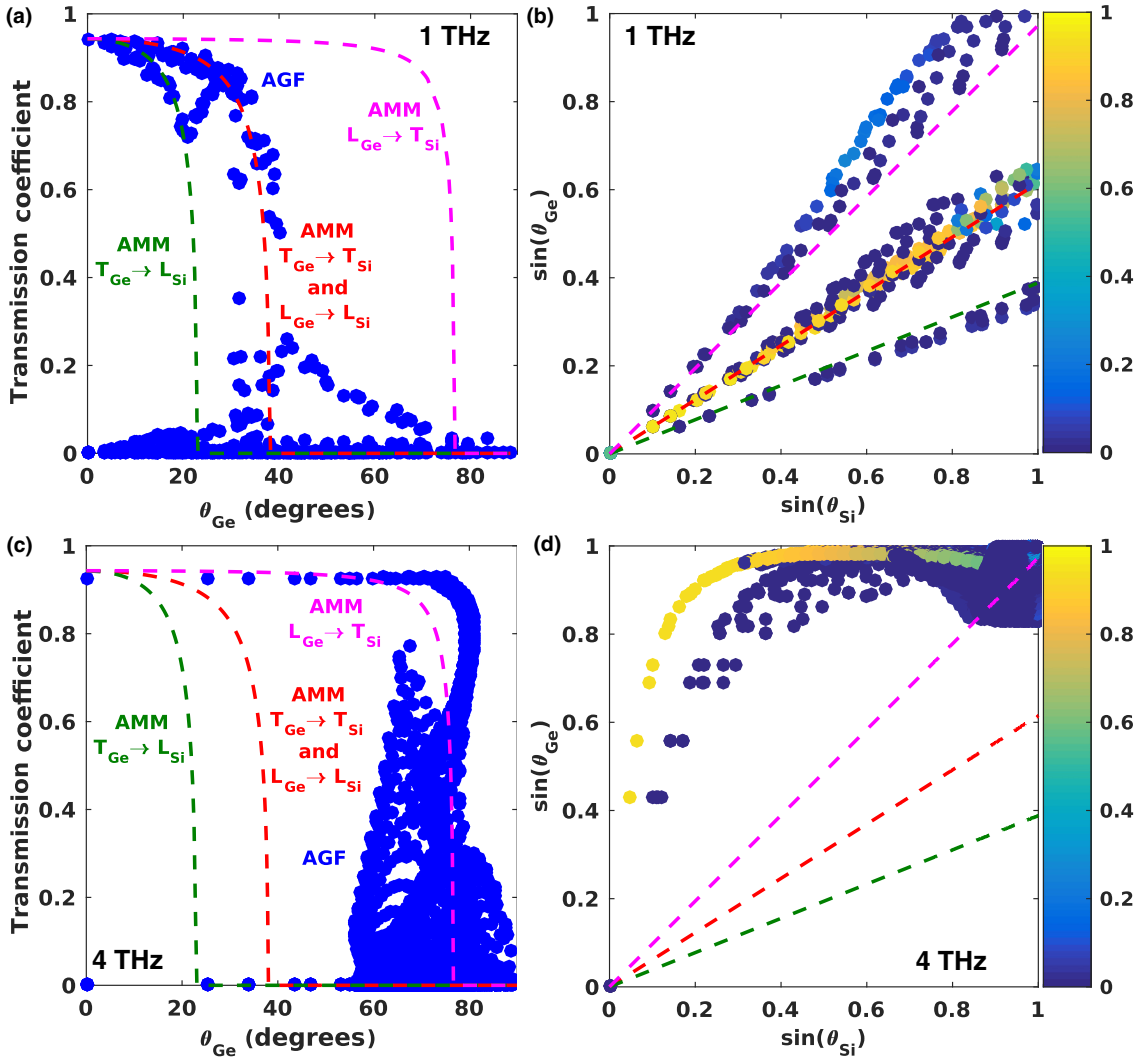

FIG. 4. Comparison between the mode-resolved AGF and the simplified AMM with either no mode conversion ($T \rightarrow T$ and $L \rightarrow L$), longitudinal to transverse conversion ($L \rightarrow T$), and transverse to longitudinal conversion ($T \rightarrow L$). (a) Transmission coefficient from Ge to Si at 1 THz. (b) Relation between the incident and transmitted angle from AGF compared with the prediction of Snell's law at 1 THz. (c) Transmission coefficient from Ge to Si at 4 THz. (d) Relation between the incident and transmitted angles from AGF compared with the prediction of Snell's law at 4 THz. The colormap represents the transmission coefficient, from 0 (dark blue) to 1 (yellow).

longitudinal phonons are converted to transverse ones ($L \rightarrow T$), and (3) transverse phonons are converted to longitudinal ones $T \rightarrow L$. Our AGF calculation naturally accounts for all these cases, enabling a comparison with the analytical predictions.

The AMM predicts the existence of critical angles θ_{cr}, above which incident phonons cannot transmit from the material with the lower speed of sound to the second one. More precisely, modes with the necessary transverse momentum do not exist in the second material and so the incident mode must be reflected. In Figs. 4(a) and 4(b), we compare the angle and transmission at 1 THz given by both theoretical frameworks. Figure 4(a) compares the transmission computed by both models from Ge to Si. Both calculations agree at such a low frequency and small incident angles, with a transmission of 0.94 consistent with the elastic wave theory. When mode conversion is not considered in the AMM, the results agree well with AGF. When transverse modes from Ge are converted to longitudinal phonons in Si, the AMM also coincides with the AGF data. However, the conversion from longitudinal phonons in Ge to transverse modes in Si is contradictory with the AGF data.

Figure 4(b) shows the sine of the angle of phonons in Ge and Si and compares them to Eq. (16) for the three cases previously described. Good agreement between the two models is depicted, showing the validity of the elastic wave theory at frequencies around 1 THz. In addition, most of the high transmission processes do not involve any mode conversion at the interface at 1 THz. To test if this simplified model can fully explain AGF data, Figs. 4(c) and 4(d) show the same comparison between the AGF and the AMM at 4 THz, where the assumptions of the AMM should be less accurate. Figure 4(c) shows that at 4 THz the trends predicted by the AMM dramatically differ from the AGF calculations. In particular, there is no critical angle above which the transmission is zero, contrary to what the AMM predicts. This discrepancy is due to the nonisotropic dispersion of

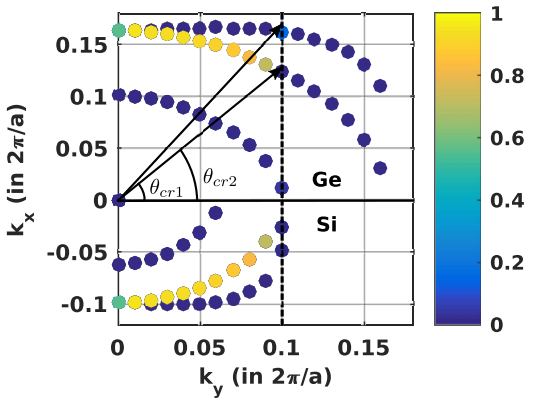

FIG. 5. Surface slowness for Ge (top half) and Si (bottom half) at 1 THz. The cross-plane component of the wave vector k_x is plotted as a function of one of the in-plane component k_y with $k_z = 0$ for each pair of coupled modes. The three acoustic branches are present in each material and two critical angles θ_{cr} appears in Ge for both transverse acoustic (TA) branches. The colormap represents the modal transmission, from 0 (dark blue) to 1 (yellow).

the actual crystals of Si and Ge that are not captured by the AMM. Figure 4(d) shows that Snell's law under the isotropic approximation no longer correctly describes the relation between the angle of phonons in Si and Ge, also due to the anisotropy of the isofrequency surface. As a consequence, the complete elastic wave theory should be applied to correctly capture the nonlinearities in the dispersion relations, which is beyond the scope of this work.

IV. ZERO-TRANSMISSION PROCESSES

An additional observation from our mode-dependent calculations is the presence of many processes with transmission coefficient of identically zero. When examining the modal transmission coefficients for a given frequency and transverse momentum, two distinct cases appear. The first case involves the presence of modes in only one lead: these modes cannot couple to phonons in the second lead due to the lack of modes with the necessary transverse momentum. In other words, these modes undergo total internal reflection.

To visualize this phenomenon, we plot in Fig. 5 the slowness surface for Ge and Si at 1 THz. The cross-plane component of the wave vector k_x is plotted as a function of one of the in-plane components, k_y, with k_z set to 0. In this figure, we distinguish three branches in Ge and Si as curves with close-to-circular shape corresponding to the longitudinal and transverse acoustic isofrequency surfaces. As the transverse wave vector k_y must be conserved at the interface, all the modes in Ge with $k_y > 0.1$ cannot couple to modes in Si, leading to total internal reflection. As a consequence, two critical angles appear for each of the transverse branches. It is worth noting that the slowness surface should be analyzed for each frequency and transverse components of the wave vector, which gives rise to many critical angles.

The second group of zero-transmission processes occurs even when modes exist in both left and right leads. In the following, we label these mechanisms as "uncoupled modes." We finally define "authorized mechanisms" as the transmission of a phonon mode from one lead to the other one with a nonzero transmission coefficient. We now investigate the fraction of processes characterized by nonzero transmission, total internal reflection, and uncoupled modes as a function of incident angle and frequency. Figure 6(a) compares these three groups with respect to frequency for phonons coming from Ge propagating towards the Si lead. At low frequency, most of the zero-transmission processes are due to total internal reflection. The large number of total internal reflection processes until 3.5 THz leads to the conclusion that it is mostly the transverse acoustic phonons that are totally internally reflected at the interface. Uncoupled mode mechanisms are

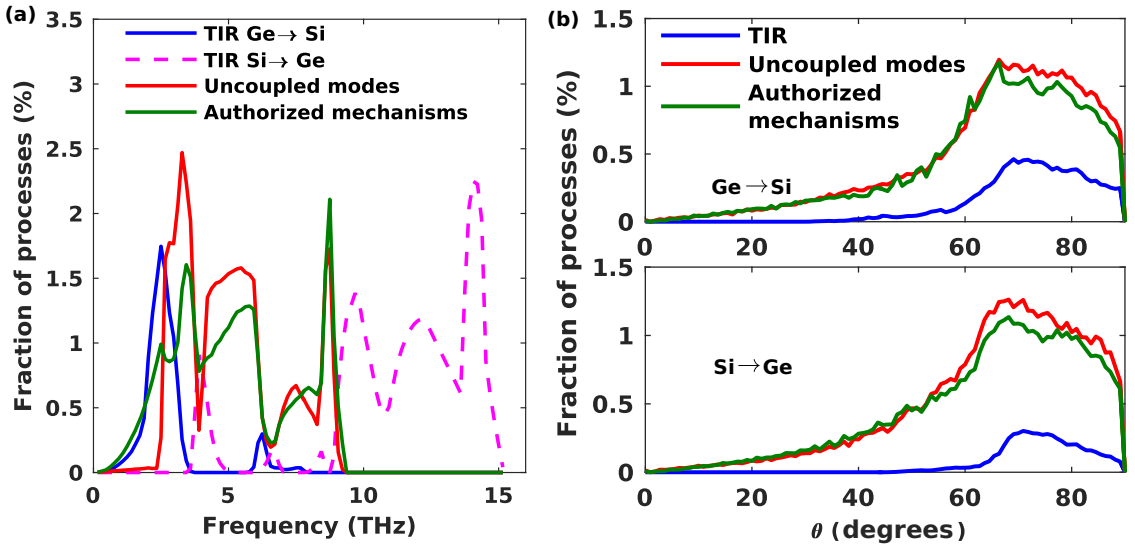

FIG. 6. Comparison of the fraction of processes involving total internal reflection (TIR), uncoupled modes, and authorized mechanisms (normalized by the total number of processes over the whole phonon spectrum). (a) As a function of frequency. TIR represents only 20% of the zero-transmission processes. (b) As a function of incident angle from Ge to Si and from Si to Ge. TIR occurs for incident angle greater at 40° in Ge and 60° in Si. Uncoupled mode processes have an angular distribution similar to that of nonzero transmission mechanisms.

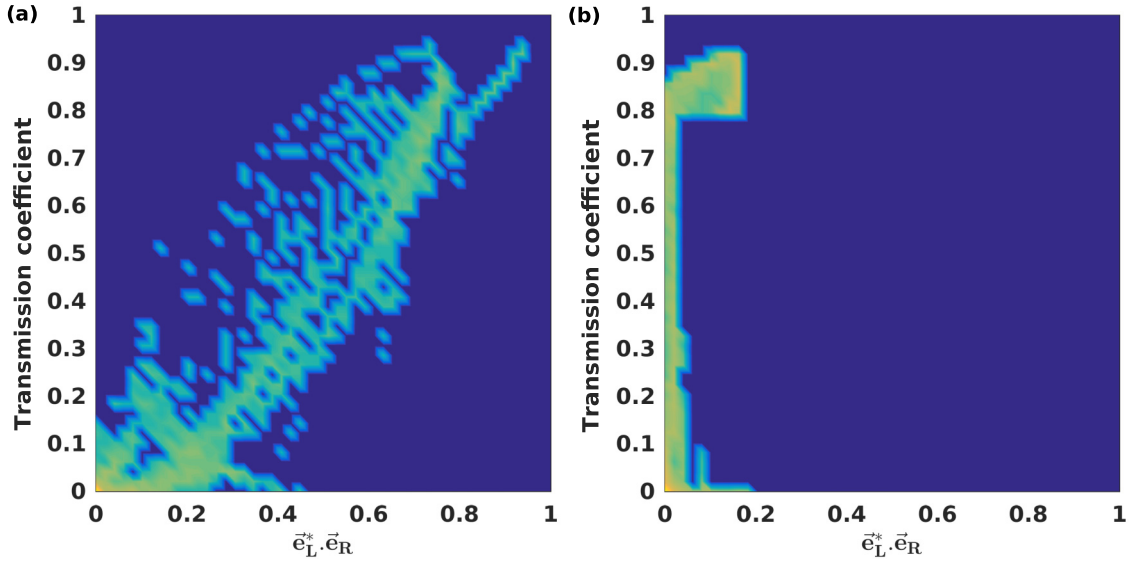

FIG. 7. Mode-resolved transmission as a function of the dot product of the left and right eigenvectors $\vec{e}^*_L \cdot \vec{e}_R$. The colormap indicates the density of processes, dark blue meaning no process and yellow indicating a high density of processes. The uncoupled mode processes cannot be explained by orthogonality of the eigenvectors.

absent until 2.3 THz, and then become as numerous as the nonzero transmission processes. Only 21% of the forbidden processes are due to total internal reflection, highlighting the importance of the uncoupled-mode processes. For frequencies lower than the cutoff frequency in the density of states of Ge, total internal reflection from Si to Ge is not the main mechanism, as predicted by the AMM. However, total internal reflection still occurs in the stiffer Si lead with higher sound velocity than Ge, showing that the anisotropic and nonlinear dispersion relations in Si and Ge can lead to unintuitive results. Naturally, above 9 THz, all the modes from Si are totally reflected as no modes are present in Ge.

The angular dependence of these processes is presented in Fig. 6(b). The two figures present a comparison for, respectively, the direction from Ge to Si and from Si to Ge. Total internal reflection processes only occur for phonons with an incident angle greater than 40° from Ge and around 60° from Si. These two angles are crucial to realize interfaces with exceptional values of TBR by taking advantage of the natural angular-dependent reflection due to the absence of modes in the second material. Uncoupled modes and nonzero transmission processes show very similar angular trends in both directions through the interface. Both trends are explained by the number of modes in each lead as a function of incident angles in Ge and Si; the number of modes at a given frequency increases as the incident angle is larger.

Although we do not know for certain the origin of the uncoupled mode processes, we suspect that symmetry considerations play a key role. For instance, it is impossible at normal incidence to excite a transverse mode from a longitudinal one. From this simple example, the orthogonality of the polarization vector in the left and right leads might play a role to explain these zero-transmission mechanisms. Figures 7(a) and 7(b) present the mode-resolved transmission as a function of the dot product $\vec{e}^*_L \cdot \vec{e}_R$, where $\vec{e}_{L,R}$ are the eigenvectors of the leads. In Fig. 7(a), a clear correlation between the mutual polarization of modes and the transmission can be drawn at 2 THz. When the vectors are aligned, a high transmission is observed. Unfortunately, this conclusion does not hold at higher frequency. Figure 7(b) shows at 8 THz that the transmission is not correlated to the dot product of the eigenvectors as $\vec{e}^*_L \cdot \vec{e}_R$ is always smaller than 0.2 and the transmission spans uniformly from 0 to 1. Thus, the eigenvector orthogonality cannot explain the physical reason of this zero-transmission group. Additional efforts will be needed to confirm that these processes are symmetry forbidden.

V. CONCLUSION

We have performed a mode-resolved study of phonon transmission through a Si/Ge interface using atomistic Green's functions with force constants from first-principles. We find that heat is carried across interfaces by a wide range of phonon frequencies and incident angles, particularly those with incident angle greater than 45°. We also show that the transmission coefficients predicted by the AMM are generally in poor agreement with the actual coefficients. Finally, we show that in addition to total internal reflection, there exists an additional major type of process with zero transmission coefficient. Even if two phonons satisfy the conservation of energy and transverse momentum at the interface, the transmission of energy by this pair of modes can still be zero. Further work is necessary to elucidate the physical origin of such processes. Our foundational work provides detailed mode-resolved insights necessary to create solid interfaces with exceptional values of thermal boundary resistance.

ACKNOWLEDGMENTS

B.L. and A.J.M. acknowledge the support of the DARPA MATRIX program under Grant No. HR0011-15-2-0039 and Boeing under the Boeing-Caltech Strategic Research & Development Relationship Agreement.

[1] D. G. Cahill, P. V. Braun, G. Chen, D. R. Clarke, S. Fan, K. E. Goodson, P. Keblinski, W. P. King, G. D. Mahan, A. Majumdar, H. J. Maris, S. R. Phillpot, E. Pop, and L. Shi, Nanoscale thermal transport. II. 2003–2012, Appl. Phys. Rev. **1**, 011305 (2014).

[2] C. Hua, X. Chen, N. K. Ravichandran, and A. J. Minnich, Experimental metrology to obtain thermal phonon transmission coefficients at solid interfaces, Phys. Rev. B **95**, 205423 (2017).

[3] R. Prasher, Thermal interface materials: Historical perspective, status, and future directions, Proc. IEEE **94**, 1571 (2006).

[4] A. J. Minnich, M. S. Dresselhaus, Z. F. Ren, and G. Chen, Bulk nanostructured thermoelectric materials: Current research and future prospects, Energy Environ. Sci. **2**, 466 (2009).

[5] G. Tan, L.-D. Zhao, and M. G. Kanatzidis, Rationally designing high-performance bulk thermoelectric materials, Chem. Rev. **116**, 12123 (2016).

[6] E. T. Swartz and R. O. Pohl, Thermal boundary resistance, Rev. Mod. Phys. **61**, 605 (1989).

[7] P. K. Schelling, S. R. Phillpot, and P. Keblinski, Comparison of atomic-level simulation methods for computing thermal conductivity, Phys. Rev. B **65**, 144306 (2002).

[8] A. Rajabpour and S. Volz, Thermal boundary resistance from mode energy relaxation times: Case study of argon-like crystals by molecular dynamics, J. Appl. Phys. **108**, 094324 (2010).

[9] Y. Chalopin and S. Volz, A microscopic formulation of the phonon transmission at the nanoscale, Appl. Phys. Lett. **103**, 051602 (2013).

[10] Y. Zhou, X. Zhang, and M. Hu, Quantitatively analyzing phonon spectral contribution of thermal conductivity based on nonequilibrium molecular dynamics simulations. I. From space Fourier transform, Phys. Rev. B **92**, 195204 (2015).

[11] W. Lv and A. Henry, Direct calculation of modal contributions to thermal conductivity via Green–Kubo modal analysis, New J. Phys. **18**, 013028 (2016).

[12] Y. Zhou and M. Hu, Full quantification of frequency-dependent interfacial thermal conductance contributed by two- and three-phonon scattering processes from nonequilibrium molecular dynamics simulations, Phys. Rev. B **95**, 115313 (2017).

[13] P. K. Schelling, S. R. Phillpot, and P. Keblinski, Phonon wave-packet dynamics at semiconductor interfaces by molecular-dynamics simulation, Appl. Phys. Lett. **80**, 2484 (2002).

[14] S. Ju and X. Liang, Detecting the phonon interference effect in Si/Ge nanocomposite by wave packets, Appl. Phys. Lett. **106**, 203107 (2015).

[15] W. Zhang, T. S. Fisher, and N. Mingo, Simulation of interfacial phonon transport in SiGe heterostructures using an atomistic Green's function method, ASME J. Heat Transfer **129**, 483 (2007).

[16] N. Mingo and L. Yang, Phonon transport in nanowires coated with an amorphous material: An atomistic Green's function approach, Phys. Rev. B **68**, 245406 (2003).

[17] D. A. Stewart, I. Savić, and N. Mingo, First-principles calculation of the isotope effect on boron nitride nanotube thermal conductivity, Nano Lett. **9**, 81 (2009).

[18] Y. Chalopin, S. Volz, and N. Mingo, Upper bound to the thermal conductivity of carbon nanotube pellets, J. Appl. Phys. **105**, 084301 (2009).

[19] Z. Tian, K. Esfarjani, and G. Chen, Enhancing phonon transmission across a Si/Ge interface by atomic roughness: First-principles study with the Green's function method, Phys. Rev. B **86**, 235304 (2012).

[20] X. Li and R. Yang, Effect of lattice mismatch on phonon transmission and interface thermal conductance across dissimilar material interfaces, Phys. Rev. B **86**, 054305 (2012).

[21] S. Ju, T. Shiga, L. Feng, Z. Hou, K. Tsuda, and J. Shiomi, Designing Nanostructures for Phonon Transport via Bayesian Optimization, Phys. Rev. X **7**, 021024 (2017).

[22] J. Mendoza and G. Chen, Anderson localization of thermal phonons leads to a thermal conductivity maximum, Nano Lett. **16**, 7616 (2016).

[23] S. Sadasivam, N. Ye, J. P. Feser, J. Charles, K. Miao, T. Kubis, and T. S. Fisher, Thermal transport across metal silicide-silicon interfaces: First-principles calculations and Green's function transport simulations, Phys. Rev. B **95**, 085310 (2017).

[24] Z.-Y. Ong and G. Zhang, Efficient approach for modeling phonon transmission probability in nanoscale interfacial thermal transport, Phys. Rev. B **91**, 174302 (2015).

[25] R. R. Kakodkar and J. P. Feser, A framework for solving atomistic phonon-structure scattering problems in the frequency domain using perfectly matched layer boundaries, J. Appl. Phys. **118**, 094301 (2015).

[26] O. Hellman and I. A. Abrikosov, Temperature-dependent effective third-order interatomic force constants from first principles, Phys. Rev. B **88**, 144301 (2013).

[27] O. Hellman, P. Steneteg, I. A. Abrikosov, and S. I. Simak, Temperature dependent effective potential method for accurate free energy calculations of solids, Phys. Rev. B **87**, 104111 (2013).

[28] D. S. Kim, O. Hellman, J. Herriman, H. L. Smith, J. Y. Y. Lin, N. Shulumba, J. L. Niedziela, C. W. Li, D. L. Abernathy, and B. Fultz, A nuclear quantum effect with pure anharmonicity causes the anomalous thermal expansion of silicon, arXiv:1610.08737.

[29] W. Zhang, T. S. Fisher, and N. Mingo, The atomistic Green's function method: An efficient simulation approach for nanoscale phonon transport, Numer. Heat Transfer, Part B **51**, 333 (2007).

[30] M. P. L. Sancho, J. M. L. Sancho, and J. Rubio, Highly convergent schemes for the calculation of bulk and surface Green functions, J. Phys. F **15**, 851 (1985).

[31] P. A. Khomyakov, G. Brocks, V. Karpan, M. Zwierzycki, and P. J. Kelly, Conductance calculations for quantum wires and interfaces: Mode matching and Green's functions, Phys. Rev. B **72**, 035450 (2005).